Macro-fiber composite actuators for a swept wing unmanned aircraft

O. Bilgen **K. B. Kochersberger** **D. J. Inman**
onurb@vt.edu **kbk@vt.edu** **dinman@vt.edu**
Virginia Polytechnic Institute and State University
Blacksburg
USA

ABSTRACT

The purpose of the research presented here is to exploit actuation via smart materials to perform shape control of an aerofoil on a small aircraft and to determine the feasibility and advantages of smooth control surface deformations. A type of piezoceramic composite actuator known as Macro-Fiber Composite (MFC) is used for changing the camber of the wings. The MFC actuators were implemented on a 30° swept wing, 0·76m wingspan aircraft. The experimental vehicle was flown using two MFC patches in an elevator/aileron (elevon) configuration. Preliminary flight and wind-tunnel testing has demonstrated the stability and control of the concept. Flight tests were performed to quantify roll control using the MFC actuators. Lift and drag coefficients along with pitch and roll moment coefficients were measured in a low-speed, open-section wind tunnel. A vortex-lattice analysis complemented the database of aerodynamic derivatives used to analyse control response. The research, for the first time, successfully demonstrated that piezoceramic devices requiring high voltages can be effectively employed in small air vehicles without compromising the weight of the overall system.

1.0 INTRODUCTION AND BACKGROUND

The design, manufacturing, and control of small unmanned air vehicles (UAVs) and micro air vehicles (MAVs) in unsteady aerodynamic loading remains an active area of research. MAVs are a class of aircraft that are small and inexpensive. They can be used for missions where larger vehicles are not practical, such as low altitude battlefield, urban, and wildlife surveillance. The fabrication of small aircraft has become more feasible with the decreased size and weight of sensors, video, communication devices, and many other electronic subsystems. However, it is known that articulated lifting surfaces and articulated wing sections actuated by servos are difficult to instrument and fabricate in a repeatable fashion on thin, composite wing MAVs. Assembly of the vehicle is complex and time consuming. Here, we examine the use of solid-state actuators to address these issues.

The past few decades have seen the development and integration of active materials into a variety of host structures as a superior means of measuring and controlling their behaviour. Piezoceramics remain the most widely used ‘smart’ or active material because they offer high actuation authority and sensing over a wide range of frequencies. A smart material, from a broad perspective, is a solid-state material that

Paper No. 3337. Manuscript received 9 August 2008, revised version received 6 March 2009 accepted 9 March 2009.

https://doi.org/10.1017/S0001924000003055 Published online by Cambridge University Press

has a transduction property between two or more fields (electrical to mechanical, thermal to mechanical, etc.). Specifically, piezoceramic materials have been extensively studied and employed in aerospace structures by performing shape and flow control. Macro-Fiber Composite (MFC) is a type of piezoceramic material that offers structural flexibility and high actuation authority. A common disadvantage with piezoceramic actuators and with the MFC actuator is that they require high voltage input. An MFC actuator could require up to 1·8kV and some active materials may require up to 10kV. In contrast, the current drain is usually low creating reasonable power consumption. The high voltage demand requires additional amplifiers and electronic circuits to be included in the system. Due to the weight of the electronic systems that come along with the active material, these actuators have been used mostly in large vehicles or in the laboratory environment. With the recent developments in electronic systems, active materials become feasible in small aircraft.

There are several benefits of using camber control via solid-state active materials as a type of morphing over the trailing edge control using conventional control surfaces. First, the low Reynolds Number (60,000 to 100,000) flow regime can result in flow separation that reduces the effectiveness of a trailing-edge control surface. Second, power-limited aircraft such as MAVs cannot afford to lose energy through control surface drag. Finally, the opportunity for flow control is inherent in the active material due to its direct effect on circulation and high operating bandwidth. The challenge is found in operating a relatively compliant, thin structure (desirable for piezo-ceramic actuators) at high dynamic pressures to extract controlling forces. Establishing a wing configuration that is stiff enough to prevent flutter and divergence, but compliant enough to allow the range of available motion is the central challenge in developing a morphing wing. The results presented here provide an example of one such design. Novel methods of mounting the actuator can take advantage of aerodynamic loads to reduce control input moments and increase control effectiveness.

Smooth control surface designs have been a research interest since the beginning of the modern aviation, the first controlled, powered and heavier-than-air flight by Wright Brothers in 1903. During the past few decades, smart materials have been implemented to control the shape of continuous aerodynamic surfaces. Smart materials have also been used in flow control by adding energy to the flow by means of synthetic jets. The following sections will list the developments in the past few decades in aerodynamic applications via smart material systems.

1.1 Smart materials in rotorcraft applications

Lazarus *et al*[1] examined the feasibility of using representative box wing adaptive structures for static aeroelastic control. A deformable typical section was utilised to derive the optimal and suboptimal relations for induced strain actuated adaptive wings. In addition, the important parameters associated with inducing curvature and twist were determined. Several important parameters were identified: The aerofoil thickness ratio, the actuation strain, and the relative stiffness ratio of the actuator to the wing skin for both camber and twist control. The stiffness coupling parameter and the wing aspect ratio were also found to be important for twist control. It was found that greater control authority along with a lower weight penalty is achievable using adaptive aeroelastic structures for a variety of wing designs. Thus, strain actuated adaptive wings may be used rather than conventional lifting surfaces to increase performance while reducing weight, decreasing loads in critical areas, improving the radar cross section, and maximising the lift-to-drag ratio for many flight conditions.

Roglin *et al*[2] presented an adaptive aerofoil that uses a shape memory alloy (SMA) actuator mechanism to actively change the camber of an aerofoil. The SMA actuators are ideal for changing the camber of the aerofoil and holding the camber change at a given configuration. Thus, the shape memory alloy induced camber changes can be used to achieve a desired collective control of the helicopter. The lift resulting from this camber change is then the primary source of the helicopter thrust replacing the conventional collective control mechanism used by a helicopter. The research demonstrated employment of the SMA actuator to generate lift for a remotely piloted helicopter.

Steadman *et al*[3] showed an application of a piezoceramic actuator in helicopter blades. Structure-control interaction was employed to develop an adaptive aerofoil that can be used in the cyclic and vibration control of a helicopter. The camber of the adaptive aerofoil can be changed by using piezoceramic actuators. The deformations produced by the piezoceramic actuators are magnified using an elastic beam that can undergo large deformations with small strains. The needed camber change can be realised over a selected band of frequencies by appropriately tuning the level of structure-control interaction.

Giurgiutiu[4] has researched improvement on rotor blades using several smart material based technologies, with the first publication in 1994. A comprehensive review paper was published in 2000. In this paper, Giurgiutiu[5] reviewed achievements in the application of smart-materials actuation to counteract aeroelastic and vibration effects in helicopters and fixed wing aircraft. A brief review of the induced-strain actuation principles and capabilities is given. Smart rotor blade applications are reviewed. Induced twist, active blade tip, and active blade flap are presented, with emphasis on experimental results. Giurgiutiu also considers the fixed wing aircraft applications. Experiments of active flutter control, buffet suppression, gust load alleviation, and sonic fatigue reduction are discussed.

1.2 Smart materials in fixed-wing platforms

Conventional or smart material actuated continuous control surface designs have also been employed in fixed-wing aircraft. Jha and Kudva[6] studied how increasing or decreasing a wing parameter affects the performance of an aircraft, demonstrating that an optimal design requires large geometric changes to satisfy a multi-role mission. A long-endurance aircraft can loiter over a target for an extended time because it utilises a high aspect ratio, unswept wing. However, this choice of planform is in direct conflict with the design of a high speed aircraft requiring a low aspect ratio, swept wing design.

Smooth cambering was applied in a Northrop Grumman unmanned combat air vehicle (UCAV) test model[7]. The unmanned aircraft demonstrated high actuation rate (80deg/sec), large deflection (20°), hingeless, smoothly contoured control surfaces with chord-wise and span-wise shape variability. Piezoelectric motors were used as actuators.

Camber control of wings using control surfaces has been extensively utilised in the industry as a morphing concept. Most of these designs use discrete and rotating leading and trailing edge controls. Trailing edge control is the more popular of the two. The F-16 Fighting Falcon uses leading-edge flaps to change the camber of the wings. In 2002, the Active Aeroelastic Wing program of NASA demonstrated twisting of wings for primarily roll control at transonic and supersonic speeds for an F/A-18 Hornet. Twist was achieved by creating aerodynamic moments on the wings by leading-edge flap and aileron deflection. The NASA-Ames Mission Adaptive Wing Research program focused on producing smooth camber change by using a flexible internal mechanism to flex the outer skin. Drag was reduced by around seven percent at the wing design cruise point, and by 20 percent at an off-design condition.

Moses *et al*[8] used both Active Fibre Composite (AFC, an earlier version of MFC) and MFC to actively reduce vibration levels in the tail fins of a wind-tunnel model of a fighter jet subjected to buffet loads. The model was tested at a Mach Number of 0·105 and a 25° angle-of-attack. One fin had five MFCs, while the other had five AFCs. Using a maximum closed-loop control signal input of 1000V to the actuators, the fin-tip peak acceleration was reduced by about 70% with the MFCs and about 85% with the AFCs at frequencies near the first bending mode. Torsional peak vibration levels were reduced 30% and 40% by delivering a closed-loop control signal to the MFCs and AFCs respectively.

https://doi.org/10.1017/S0001924000003055 Published online by Cambridge University Press

Along with the developments listed above, inflatable wings were mostly developed within the last few decades. Aspects of inflatable technologies and a review of inflatable wing and related technologies is included in Cadogan *et al*[9,10]. More recent interest in inflatable wings was demonstrated through the development of an inflatable wing UAV for NRL by Vertigo, Inc. Flight tests of deployment and low-altitude flight of the design were conducted in 2001 by researchers at NASA Dryden[11]. The skeleton of the wing was made of inflatable tubes, surrounded with crushable foam to provide the aerofoil cross-section. After the aircraft was released, the five-foot span inflatable wing was successfully deployed in about one-third of a second. To maintain strength and stiffness of the wing, nitrogen gas pressurisation of 300psi was required.

Simpson and Jacob[12] presented research on developing UAVs using inflatable wings with wing warping for roll control. The inflatable wings are constructed with internal bladders and flexible external restraints and inflatable wing stiffness varies with internal pressure, which is required for operation. The research focused on characterising the deformation of the wings and developing a model to accurately predict this deformation and the resulting aerodynamic performance. Laboratory investigations of wing warping are presented and discussed, as well as flight tests of a small-scale UAV with inflatable wings using wing warping roll control.

In recent years, several important advances have been centered on squeezing more performance out of existing adaptive materials and enhancing the performance of materials yet to come. Post Buckled Precompression (PBP) concept, in its earliest incarnation was primarily intended to increase the coupling coefficient exhibited by piezoelectric transducer elements[13]. Experimental testing showed that apparent coupling coefficients approaching one could be achieved by axially loading bending elements with forces that approached the buckling load of the beam. Vos *et al*[14] conducted research to improve the PBP concept for aerodynamic applications. In this work, the design, modeling, and testing of a morphing wing for flight control of an uninhabited aerial vehicle is presented. Axial precompression was generated in the piezoelectric elements by an elastic skin which covered the outside of the wing and served as the aerodynamic surface over the aft 70% of the wing chord. A two-dimensional semi-analytical model based on the Rayleigh–Ritz method of assumed modes was used to predict the static and dynamic trailing-edge deflections as a function of the applied voltage and aerodynamic loading. It was shown that static trailing-edge deflections of ±3·1° could be attained statically and dynamically through 34Hz. Wind-tunnel and flight tests showed that the PBP morphing wing increased roll control authority on a 1·4m span uninhabited aerial vehicle while reducing weight, slop, part-count, and power consumption.

Seigler *et al*[15] focused on modeling and flight control of large-scale planform altering flight vehicles. The equations of atmospheric flight are derived in a general form, methods of integrating the aerodynamic forces are examined, and various approaches and methods of flight control are distinguished.

1.3 Flow control with smart material actuators

The use of conformal, zero mass flux actuators in aerodynamic flow control has been presented recently as a novel means of controlling laminar separation bubble (LSB) on small aircraft subjected to low Reynolds Number flows. Conformal zero mass flux actuators include synthetic jets[16], plasma actuators[17] and piezo-ceramic actuators that move in the out-of-plane direction[18]. The motivation for designing such an actuator is to increase the bandwidth of actuation, where the ability to re-attach the LSB is dependent on the excitation frequency. Mechanical actuators are limited in frequency due to mass loading effects while the MEMS actuators can operate at orders of magnitude higher frequency. There are also non-zero mass flux trailing edge blowing (TEB) for circulation control, demonstrated in applications from helicopters[19] to turbine blades. The complexity and weight of TEB actuators make them a poor choice for small aircraft applications where size, weight and power are primary concerns.

Acharya[20] presented the application of flow control technology to the compressor of a gas-turbine engine designed for UCAV applications are described. 'Smart' stator vanes and inlet guide vanes (IGVs) were developed and demonstrated in research compressor rigs. Flow-control modules were incorporated on the suction surface of stator vanes to delay or eliminate flow separation in the vane passage, thereby enabling higher vane loadings, and in the trailing-edge region of IGV aerofoils to vector the flow leaving the vane row to desired flow angles. These modules were based on pulsed-blowing and trailing-edge-blowing approaches respectively. The actuation technologies, actuators, flow-state sensing, signal processing, and control algorithms required for closed-loop actuation of the vane flow-control systems were developed and tested.

Santhanakrishnan *et al*[21] discussed several technologies currently being investigated for use on low speed UAVs. This includes adaptive wing technology that controls separation via active changes in the camber, use of large scale surface roughness to control separation, plasma actuators to control stall and enhance lift, and inflatable wings that can be tailored using wing warping. In the study, THUNDER piezoelectric actuators are employed in a cavity on the wing. The entire assembly is wrapped in a latex membrane to hold it together and provide a seamless outer surface. The actuator oscillation changes the profile of the suction surface by about one percent of chord.

Gomes[22] investigated on the effect of geometry and actuation variables on peak jet velocity of a piezoelectric diaphragm synthetic jet actuator using hotwire anemometry. Two distinct experiments were conducted; the first at constant excitation amplitude with the aim of identifying the SJA geometry that provides the highest jet velocity. This geometry was then used in a second experiment with constant geometry to explore the effects of excitation amplitude on actuator jet velocity.

Patel *et al*[23] presented the use of dielectric barrier discharge plasma actuators for hingeless flow control over a 47° 1303 UCAV wing. Control was implemented at the wing leading edge to provide longitudinal control without the use of hinged control surfaces. Wind-tunnel tests were conducted at a chord Reynolds Number of 412,000 and angles of attack ranging from 15° to 35° to evaluate the performance of leading-edge plasma actuators for hingeless flow control. Operated in an unsteady mode, the actuators were used to alter the flow field over the lee-side wing to modify the aerodynamic lift and drag forces on the vehicle. When compared with the conventional trailing-edge devices, the plasma actuators demonstrated a significant improvement in the control authority in the 15° to 35° angle-of-attack range, thereby extending the operational flight envelope of the wing. The study demonstrated the technical feasibility of a plasma wing concept for hingeless flight control of air vehicles, in particular, vehicles with highly swept wings and at high angles of attack flight conditions in which conventional flaps and ailerons are ineffective.

1.4 Morphing in small unmanned aircraft

Continuous morphing concepts have also been utilised in smaller air vehicles. The researchers at the University of Florida have developed a series of MAVs that incorporate a unique, thin, reflexed, flexible wing design[24-27]. There is some evidence that the flexible wing design reduces adverse effects of gusty wind conditions and unsteady aerodynamics, exhibits desirable flight stability and enhances structural durability. The wings are constructed of a carbon fibre skeleton and a thin flexible latex membrane.

Garcia *et al* investigated the use of morphing to provide control authority[28]. A torque tube actuated by servos twisted or curled the flexible wing. Flight tests show that wing twisting or curling was a good strategy to command roll manoeuvres. The vehicles were easy to fly and were suitable for autopilot control. The aerodynamic characteristics of isolated MAV wings and complete aircraft are considered a good base study for general aerodynamic considerations and a necessary step for a sound MAV wing design.

https://doi.org/10.1017/S0001924000003055 Published online by Cambridge University Press

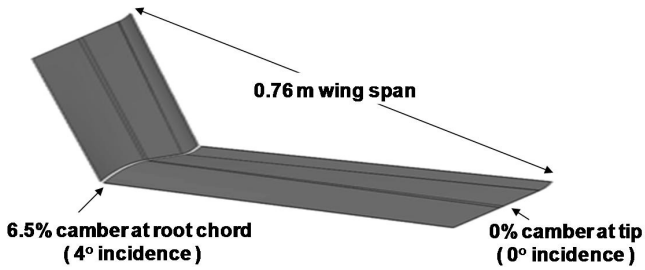


Figure 1. Final design of the wings. The camber of the reflex at the trailing-edge is constant along the span.

Table 1
Specifications for aircraft used in flight tests

Overall Specifications		Weight Distribution, [grams]	
Weight:	0.815 kg	Battery:	106
Wingspan:	0.76 m	Power Electronics:	103
Wing Chord:	0.15 m	Other Electronics:	99
Wing Sweep:	30 degrees	Wings:	168
Cruise Speed (approx.):	17.5 m/s	Main Frame:	263
Re_{chord}:	$1.7 * 10^5$	Rest of the Vehicle:	76
Power Consumption, [Watt]		**Moment of Inertia, [kg*m^2]**	
Motor (at cruise speed):	150	I_{roll} (at CG):	$1.02 *10^{-2}$
Smart Actuators and Power Circuit (max.):	3	I_{yaw} (at CG):	$1.40 *10^{-2}$
		I_{pitch} (at CG):	$6.81 *10^{-3}$

Kim and Han designed and fabricated a smart flapping wing by using a graphite/epoxy composite material and an MFC actuator[29]. This study was aimed to mimic the flapping motion of birds. Wind-tunnel tests were performed to measure the aerodynamic characteristic and performance of the surface actuators. A test stand was also designed to measure the lift and thrust generated by the flapping device. The tests were done on a commercial ornithopter named Cybrid-P2 with and without the MFC actuator. A twenty percent increase in lift was achieved by changing the camber of the wing at different stages of flapping motion.

1.5 Air vehicle control using Macro-Fiber Composite actuators

Piezoceramics have been used in many applications due to their high frequency bandwidth. In many cases, the piezoceramics are brittle, making them impractical for direct shape control. Macro-Fiber Composites were developed at NASA Langley Research Center[30]. An MFC is a flexible, planar actuation device that employs rectangular cross-section, unidirectional piezoceramic fibres (PZT 5A) embedded in a thermosetting polymer matrix. This active, fibre reinforced layer is then sandwiched between copper-clad Kapton film layers that have an etched interdigitated electrode pattern. A comprehensive manufacturing manual for MFC can be found in High and Wilkie[31]. The in-plane poling and subsequent voltage actuation allows the MFC to utilise the d_{33} piezoelectric effect, which is much stronger than the d_{31} effect used by traditional PZT actuators with through-the-thickness poling[32]. MFC has a uniform geometry, including PZT fibre and electrode spacing and continuity, as well as the absence of air voids or particulate inclusions. There has been extensive analytical and experimental research focused on utilising MFC as an actuator (or sensor) for structural control. Williams[33] provides a detailed nonlinear characterisation of the mechanical and piezoelectric behaviour of the MFC actuator.

Bilgen *et al*[34] recently presented static flow vectoring via MFC actuated thin aerofoils. Wind-tunnel experiments and theoretical analysis is conducted on a 1·15% thick, 54mm chord, and 108mm span composite aerofoil. Wind-tunnel results and theoretical evaluation of the aerofoils show comparable effectiveness to conventional actuation systems. Deformation of the aerofoils due to pressure distribution is studied by finite element method. All concepts present adequate stiffness for flow speeds up to 30ms^{-1}.

The high strain and high structural deflection requirement under aerodynamic loads creates the need for semi-solid-state mechanisms to be employed along with piezoceramic actuation. Bilgen *et al*[35] used MFC actuators in a novel, variable camber aerofoil design to understand the behaviour of solid-state aerodynamic vectoring in high dynamic pressure air flow. The study focused on kinematical modeling, and theoretical static response characterisation under aerodynamic loads. The aerofoil was designed to provide bi-directional aerodynamic vectoring. The design employs two MFC actuated bimorph laminates in the top and bottom surfaces of the aerofoil. A compliant parallelogram (box structure) allows the desired leading-edge path with given input voltage. For demonstration of the concept, a prototype is constructed which produced deflection in both directions from a flat camber line. The box mechanism amplifies the deflection and camber change as predicted. The concept outputs approximately 15mm deflection at the trailing edge for maximum positive voltage, and –18mm deflection at the trailing edge for maximum negative voltage. The trailing edge is 90mm from the closest side of the box structure. Theoretical analysis showed increase in lift-over-drag when compared to thin, flat plate aerofoil designs.

The purpose of the research presented here is to exploit MFC actuation to perform shape control of an aerofoil on a small aircraft and to determine the feasibility and advantages of smooth control surface deformations. Continuous camber generation, instead of an articulated surface, is employed as a morphing strategy. The next section presents the experimental aircraft design and the computational model. Next, wind-tunnel tests are presented and results are compared to the previously published values. The following section presents the flight test data and an analysis of the flight video. The paper concludes with the summary of results and discussion of future work.

2.0 AIR VEHICLE DESIGN AND THEORETICAL ANALYSIS

A test platform for the MFC actuated morphing wing concept was developed to demonstrate the feasibility and the control authority of the piezo-composite actuators. A remotely piloted, thin composite wing aircraft provided a durable, lightweight platform for testing the concept. A swept, 'flying wing' planform with two MFC patches was chosen as the design backbone. A thin aerofoil was adapted to maximise the camber change induced by the MFC actuators. In theory, actuation of the MFCs in the same direction causes pitch and actuation in opposition causes roll due to the planform configuration. MFC 8557 P-1 actuators, 85mm long and 57mm wide, were placed 0·31m from the root chord of the wing to increase roll moment due to change in camber of the aerofoil. Details of the vehicle can be found in authors' previous work[36]. The aerofoil design has 6·5% constant camber on its major curvature for the root section. This camber is linearly reduced from root to tip from 6·5% to 0% camber. The outboard section of the composite wing is designed so that maximum actuation of the MFC would bring the outer wing section camber to the same camber as the root section. The 30° swept wing design shown in Fig. 1 has a 4° incidence at the root which gradually decreases to zero degree towards the tip.

In addition to the variable camber wing surfaces, the aircraft was equipped with a rudder (25mm wide and 76mm tall) and an elevator (203mm wide and 51mm deep). They served to mitigate risk during test flights and provided 'excess' control authority to ensure safe test flights.

https://doi.org/10.1017/S0001924000003055 Published online by Cambridge University Press



Figure 2. Fabricated vehicle employing two MFC 8557-P1 type actuators.

2.1 Electronics

The aircraft electronics are typical for model aircraft except for the power electronics that drive the MFC actuators. Remote communication was achieved using a 72MHz radio transmitter and receiver combination. An 11·1V Lithium-Polymer (Li-Po) battery was used to power all electronics on-board. A 150 Watt brushless motor generated thrust. Two servo actuators were used to trim yaw and pitch. MFC patches were controlled and powered through a series of converters.

2.2 MFC power electronics

Due to the nature of piezoceramics, a high voltage power supply was necessary on-board. Two T1505 DC-DC converters from AMI Electronics were used to supply 0 to 1,500V to the MFC patches. These converters receive 0 to 5V input and output 0 to 1,500V proportional to the input. Maximum power output is 1 Watt per converter. Two RC-DC converters from CK Design Technology were used to translate pulse-width-modulation (pwm) signals from the receiver to an analogue DC signal output to the DC-DC converters. A power booster circuit was used to amplify current output capability of the RC-DC converter to the DC-DC converter. The MFCs and the power electronics consume approximately 3·0 Watts during maximum (symmetric) actuation.

2.3 Overall specifications of the aircraft

Table 1 summarises overall aircraft specifications. The final aircraft weighed significantly more than the initial design. The weight increase was due to design modifications along the fabrication process. The increased weight also required a higher cruise speed and also higher cruise incidence angle.

One of the benefits of the thin, composite wing is its low moment of inertia. The low moment of inertia of the aircraft allows a sufficient roll response with lower control surface loads. In the case of the current variable-camber aircraft, this translates lower voltage actuation of the MFCs. The fabricated aircraft can be seen in Fig. 2.

The final design has a 0·76m wingspan and approximately 0·815kg total weight. All electronics, including MFC power electronics (103 grams), are powered by an 11·1V Lithium-Polymer battery (106 grams), a common choice for remotely controlled aircraft. The MFC 8557-P1 type actuators weigh approximately eight grams each. Although a direct comparison to a conventional (servo controlled) aircraft is impractical, two servo motors weighing approximately 37 grams would be used in a radio controlled (RC) vehicle with the same size and weight. The aircraft uses a 150W brushless motor for thrust; in contrast the MFC power electronics consume only 3·0 Watts during maximum actuation.

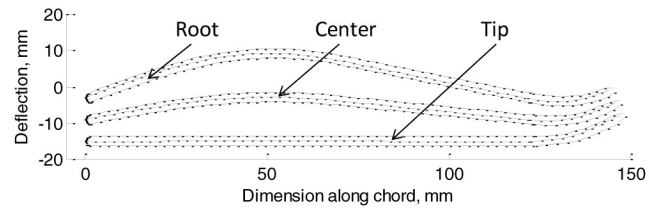


Figure 3. Wing section geometry for root to tip for no MFC actuation.

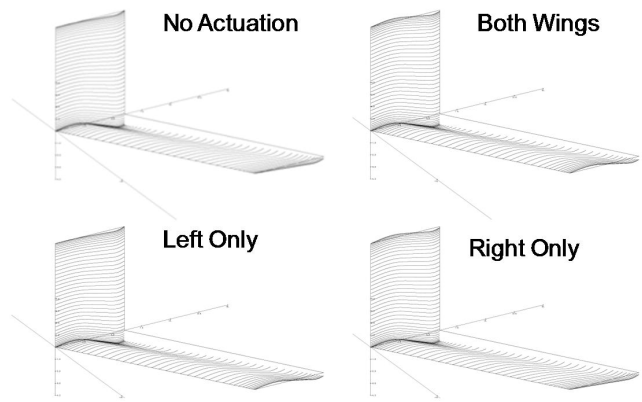


Figure 4. Wing geometries for all operational conditions tested.

2.4 Vortex lattice model of the aircraft

A preliminary analysis is conducted to evaluate the effectiveness and the stability of the wing design before the wind-tunnel and flight tests. The aircraft is modeled using vortex lattice software Athena Vortex Lattice (AVL)[37]. AVL is well suited for aerodynamic configurations which consist mainly of thin lifting surfaces at small angles of attack and sideslip. These surfaces and their trailing wakes are represented as single-layer vortex sheets, discretised into horseshoe vortex filaments, whose trailing legs are assumed to be parallel to the streamwise axis. AVL provides the capability to also model slender bodies such as fuselages and nacelles via source+doublet filaments. Since the fuselage is expected to have little influence on the lift and roll response, it is left out of the model. AVL assumes quasi-steady flow, meaning that unsteady vorticity shedding is neglected. It also assumes that any oscillatory motion (in roll or in pitch) must be slow enough so that the period of oscillation is much longer than the time it takes the flow to traverse an aerofoil chord. This is true for virtually any expected flight maneuver that is observed in the current vehicle. Also, the roll, pitch, and yaw rates used in the computations must be slow enough so that the resulting relative flow angles are small. It must be noted that AVL only predicts the induced drag portion of the total drag. The theoretical induced drag is reported in the following section to define a lower bound on the actual drag generated by the wings. A cosine chordwise and spanwise distribution is chosen for discretisation of the geometry into vortex lattice panels. The cosine spacing is generally the most efficient distribution (best accuracy for a given number of vortices). The strips are concentrated at the leading edge (LE) and trailing edge (TE) along the chordwise direction and at root and tip along spanwise direction. Each wing is divided into 40 sections in the spanwise direction and 20 sections in the chordwise direction due to complex geometry produced by aerofoil section and the spanwise twist and sweep angle. Section geometries that are used in AVL model from root to tip are shown in Fig. 3 for wing under no MFC actuation.

The thin aerofoil sections are given a 1·7% thickness ratio with circular LE geometry and a finite TE gap. Spanwise geometry is linearly interpolated in between the tip and root section profiles.

https://doi.org/10.1017/S0001924000003055 Published online by Cambridge University Press

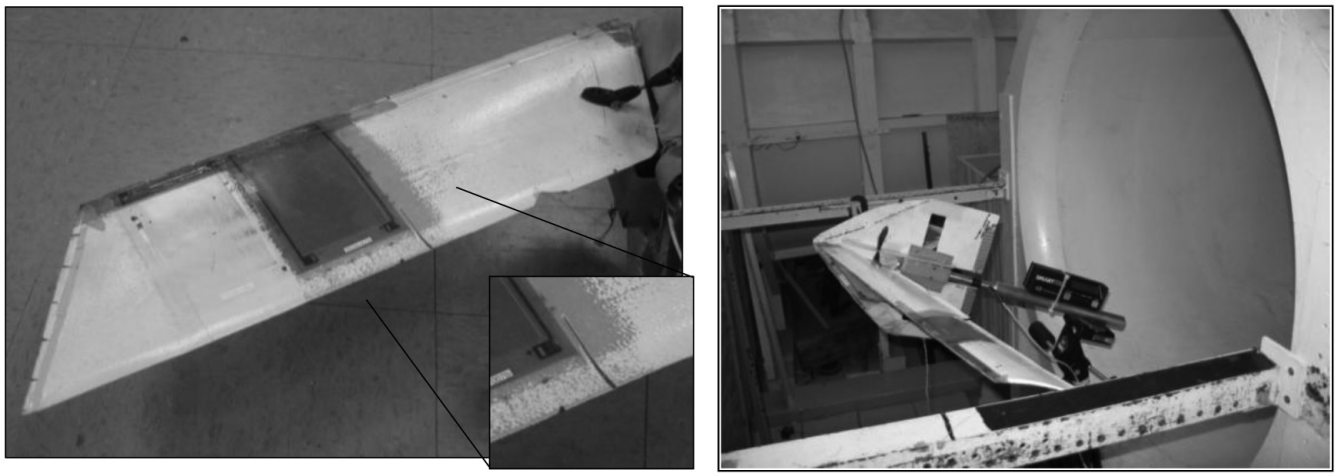


Figure 5. Left: Left wing (modified) with two MFC actuators. 50mm cut on the TE relieves inboard section constraint. Right: Test aircraft (with modified wings) on the wind-tunnel sting balance.

These profiles represent the actual geometry of the wing in a wind-off condition. The vortex-lattice code does not take any aeroelastic effects into consideration. Figure 4 shows the geometry definition for each operational case. The main frame is also modeled however is not shown in the figure. Four operational conditions are evaluated: No actuation, both wings actuated, right wing only and left wing only cases.

The geometry used in the model is representative of the fabricated vehicle. Due to fabrication and assembly of the vehicle, the root and tip incidence angles were slightly off from the CAD model. The spanwise camber and twist values also included a small offset. These parameters were measured during wind-off condition and AVL model was updated. The AVL results, for a range of 0-10 degree AOA (where the VL method is accurate), will be presented along with the wind-tunnel results in the following section. The geometric differences between the wings are demonstrated in the aerodynamic response from both experiments and computational evaluation. Also, the theoretical results represent a configuration without any aeroelastic effect, which serves as a baseline and the desired response. The comparison is given to identify of the additional effects (if any) due to the fluid-structure interaction. It must be noted that only wings and main-frame (vertical plane) is modeled in AVL, and the model is representative the actual geometry used in the wind-tunnel experiments.

3.0 WIND–TUNNEL EXPERIMENTS

The performance of the variable-camber wings were quantified by wind-tunnel experiments conducted at the Virginia Tech Aerospace and Ocean Engineering open section closed loop low-speed wind tunnel. This tunnel has a 0·9m diameter jet into an open section, allowing easy access for mounting and configuring instrumentation. Previous wind-tunnel experiments[38] on the morphing wings were limited to lift, drag and roll information. The experimental evaluation given in this paper covers detailed lift, drag, roll and pitch characteristics for four operational conditions: 'No Actuation,' symmetrically 'Both Wings' actuated, and the two asymmetric cases, 'Right Wing' only, and 'Left Wing' only.

Unlike the flight test article given in the previous section, which had one MFC patch installed on each wing, two MFC patches were mounted on each wing to ensure adequate control power would be achieved for the sting balance. Previous examination of structural characteristics[38] revealed less-than-desired camber change and also reduction in LE incidence with applied voltage. These two effects resulted in a lower force and moment outputs. Two solutions were employed in the current study: 1) A thin glass/epoxy layer was bonded to LE of both wings to make it stiffer in the spanwise direction. 2) To increase the change in camber due to MFC actuation, the trailing edge of the wings were cut in the chordwise direction. The second modification allowed MFC actuated outboard section of the wing to have less constraint enforced by the inboard section. This discontinuity theoretically causes a small amount of drag addition which will be discussed later. Figure 5 shows the modified wings and the wind-tunnel aircraft with four MFC actuators.

The electronics were removed from the aircraft to avoid exceeding the static force limits of the sting balance, however the fuselage was left on to represent actual aerodynamic characteristics. A NASA LaRC sting balance, GA-10, rated at maximum 40N normal, and 13N axial force and 3·1Nm pitch, and 0·89Nm roll moment, was used to measure forces and moments. The strain gage bridge amplifier was connected to a National Instruments cDAQ data acquisition system with eight 16 bit input channels, allowing user-defined sample rates and periods for each run. The elevator was removed to allow attachment of the balance. The actuation of the MFC patches was done using a Trek 50/750 high voltage amplifier.

Measurements were done at 0 to 24 degrees of angle-of-attack in 2 degree increments. For each AOA, the constant voltage (1,500V) was applied symmetrically (both wings) and asymmetrically (left wing only, right wing only). The case with zero voltage was also measured as baseline. Symmetric actuation was conducted to reveal lift, drag and pitch characteristics, whereas asymmetric actuation was conducted to show roll characteristic of the aircraft. Note that MFC actuators can be actuated within a –500V to 1,500V range. Since the negative actuation created additional complexity to the test routine, only 0V and 1,500V actuation were considered.

3.1 Force and moment calculations

The equations relating balance loads and moments to aircraft loads and moments are given by:

$$\begin{aligned} L &= F_N \cos(\alpha) - F_A \sin(\alpha) \\ D &= F_N \sin(\alpha) + F_A \cos(\alpha) \\ M_X &= M_{BX} \\ M_Y &= M_{BY} - F_N Xref \end{aligned} \quad \ldots (1)$$

where F_N, F_A are the measured normal and axial forces, and M_{BX}, M_{BY}

https://doi.org/10.1017/S0001924000003055 Published online by Cambridge University Press

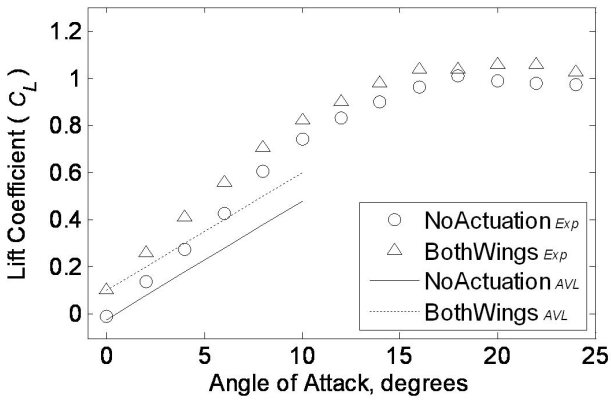


Figure 6. Lift coefficient comparison at 10·5ms^{-1} Re$_c$ = 1·01E5.

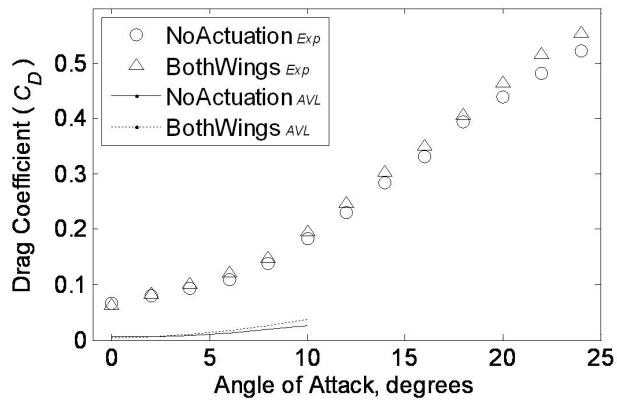


Figure 7. Drag Coefficient comparison at 10·5ms^{-1}. Re$_c$ = 1·01E5.

are measured roll and pitch moments respectively. L and D are the calculated lift and drag forces and M_X and M_Y are roll and pitch moments respectively. Angle-of-attack, α, was measured using a SmartTool digital inclinometer, with all angles referenced to the aircraft thrust axis. X_{ref} is the distance between the pitch-moment center of the balance and the reference point on the test aircraft. The aerodynamic center of the two wings is chosen as the reference point which is located 0·146m from the LE of the vehicle.

As reported in authors' previous work[36], the aerodynamic loading of a 2D wing section morphed with MFC actuators results in a camber decrease of approximately 0·03% for a speed of 15·4ms^{-1} at zero degree incidence. An average decrease of 0·033%camber/deg was also noted with increasing AOA. Since it was impractical during the wind-tunnel tests (wind-on conditions) to measure actual camber values due to a low-amplitude torsional limit cycle, the measured camber change during wind-off conditions will used with the modifications from the data in Ref. 36. Lift, drag and moment coefficients were computed using:

$$C_L = L/(0{\cdot}5\rho S u^2)$$
$$C_D = D/(0{\cdot}5\rho S u^2) \quad \ldots (2)$$
$$C_l = M_X/(0{\cdot}5\rho S b u^2)$$
$$C_m = M_Y/(0{\cdot}5\rho S c u^2)$$

based on a wing area of S = 0·118m^2 , wingspan of b = 0·76m and chord of c = 0·15m. The absolute pressure of 951·2hPa and average temperature of 19·5°C was measured in the laboratory. Using the ideal gas law, density of air was calculated to be ρ = 1·13kgm^{-3}. Air velocity, u, was calculated by applying Bernoulli's equation to the Pitot-Static tube. The pressure difference across the Pitot-Static tube was recorded with the Setra 267 pressure transducer for each run. An average air velocity of 10·5ms^{-1} was calculated.

3.2 Uncertainty analysis

In computing 95% confidence limits on the data, the uncertainty of measured forces and moments had to be determined. Using AIAA Standard[39], both precision (P) and bias (B) errors were considered. Bias error estimates were based on repeatability during the sting balance calibration. The following bias errors were determined using nominal aircraft forces and moments: B_L = 0·23N, B_D = 0·15N, B_{MX} = B_{MY} = 0·052Nm. Total error in the force and moment measurements was then computed as follows:

$$U = \sqrt{P^2 + B^2} \quad \ldots (3)$$

The precision errors are based on (95% confidence band) values obtained from runs over a 20 second period. In obtaining force and moment coefficients, the uncertainties in dynamic pressure (Q), measured wing area (S), wingspan (b) and chord (c) also contribute to the overall uncertainty. Using the method of Kline-McClintock, the force (F) and moment (M) coefficient uncertainties were calculated. The force coefficient uncertainties become:

$$U_{C_F} = C_F\sqrt{\left(\frac{U_F}{F}\right)^2 + \left(\frac{U_Q}{Q}\right)^2 + \left(\frac{U_S}{S}\right)^2} \quad \ldots (4)$$

and the moment coefficient uncertainties become:

$$U_{C_M} = C_M\sqrt{\left(\frac{U_M}{M}\right)^2 + \left(\frac{U_Q}{Q}\right)^2 + \left(\frac{U_S}{S}\right)^2 + \left(\frac{U_{(b,c)}}{(b,c)}\right)^2} \quad \ldots (5)$$

Calculated uncertainties for each angle-of-attack are presented in Table 2. The increase in uncertainty as the angle-of-attack is increased is most likely due to the building of limit cycle vibration that was observed at the wing tips during testing.

3.3 Wind-tunnel test results and comparison to AVL model

The wind-tunnel test series produced lift, drag and moment coefficients. The C_L *vs* α data is shown in Fig. 6, plotted for the maximum tip camber condition (2·6%) at 1500 volts, and the minimum tip camber condition (0·3%) at zero volts. With an aspect ratio of four, the theoretical maximum lift curve slope is $C_{L\alpha,Theory}$ = 0·073/deg, neglecting wing sweep. AVL predicts $C_{L\alpha,AVL}$ = 0·051/deg for the aircraft. The measured average value of $C_{L\alpha,Exp}$ = 0·078/deg is higher than the theoretical value due to separated flow on the bottom of the aerofoil re-attaching at higher angles, causing a steeper lift gradient between three and eight degrees angle-of-attack. This behaviour is common on thin aerofoils and has been reported in Ref. 40. Previous wind-tunnel experiments showed a $C_{L\alpha,old}$, of 0·06. This confirms that the

Table 2
Absolute uncertainties for force and moment coefficients

AOA	UCL	UCD	UCl = UCM
0	1.82E-02	1.08E-02	4.11E-03
4	1.45E-02	7.04E-03	4.38E-03
8	2.42E-02	2.12E-02	3.26E-03
16	5.91E-02	6.14E-02	3.32E-03
24	1.02E-01	1.58E-01	1.69E-02

https://doi.org/10.1017/S0001924000003055 Published online by Cambridge University Press

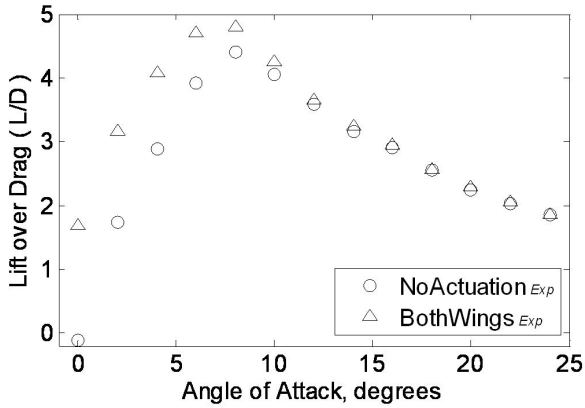


Figure 8. Experimental Lift / Drag comparison at 10·5ms^{-1}. Re$_c$ = 1·01E5.

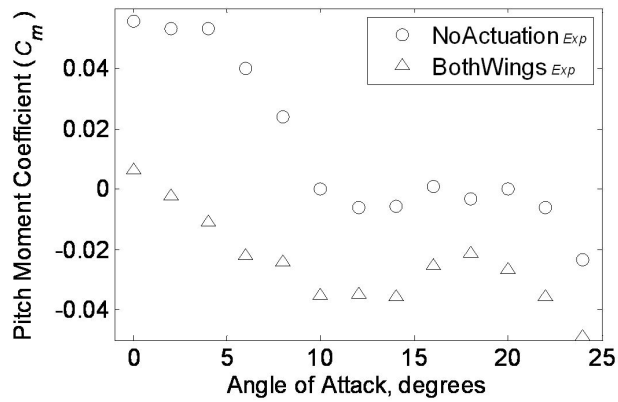


Figure 9. Pitch Moment Coefficient comparison at 10·5ms^{-1}. Re$_c$ = 1·01E5.

modifications made to the wings improved the lift characteristics. The maximum lift coefficient of C_{Lmax} = 1·06 is also higher than the previously recorded C_{Lmax} = 0·83. Assumptions about the camber deflection when 'cruise' voltages are applied on the MFC patches turned out to be optimistic, with the wing tips showing only a change of 2·3% camber when full voltage is applied. This resulted in a less-than-optimal wing shape at cruise conditions.

The C_D *vs* α curve is shown in Fig. 7. One of the main benefits of the morphing control is that the overall drag does not increase significantly during pitch and roll control deflections, typical of conventional controls. For small aircraft that are subjected to turbulence, control deflections are large and frequent, and so reductions in drag become important.

The drag at zero degree AOA for the current test is $C_{D,min}$ = 0·06 for both actuated and un-actuated configuration. In comparison to the previously reported drag coefficient (without the cut on the wings) there is no conclusive addition of drag induced by the chordwise discontinuity on the wings caused by the cut. The drag coefficient is significantly higher than predicted, for all AOA range tested, due to several reasons. As mentioned in the previous section, the AVL prediction of the drag is limited to induced drag. Also, the fuselage is a major source of drag, which is not modeled in AVL. In addition, the vertical body (shown in Fig. 2) has a blunt leading edge. An aerodynamic improvement of the fuselage and the vertical body will cause a significant reduction in drag which is not addressed here.

The *L*/*D vs* α curve is shown in Fig. 8. The max *L*/*D* within flight incidence range is 4·79 which is higher than previously reported value of 3·0. The benefit of camber control is observed here, where performance improves when camber is increased to affect a rolling or pitching maneuver. The prototype aircraft design showed considerable parasite drag resulting in the relatively low *L*/*D* when compared to other aircraft in its size and weight category. Three sources of drag were identified: the thin aerofoil design promotes separation at the leading edge, limit cycle oscillations were observed on the outer half span during most test conditions, and the fuselage has not been adequately faired. All of these sources of drag can be addressed without compromising the morphing effect, improving the aircraft performance.

The lift authority of the camber actuation is decreased as AOA is increased. In contrast, the drag authority is increased with higher AOA. The change in *L*/*D* due to actuation decreases from $\Delta L/D_{\alpha=0^\circ}$ = 1·97 to $\Delta L/D_{\alpha=24^\circ}$ = 0·29. In summary, the effectiveness of camber actuation is reduced with increasing AOA.

The pitch moment coefficient, C_m *vs* α is presented in Fig. 9. The aerodynamic center of the wings is considered as the reference point for pitch moment calculations. The aerodynamic center is 0·146m from the LE of the aircraft. The experimental results showed an average negative slope.

The pitch moment slope with increasing angle-of-attack has a negative slope until 10° and beyond 18°. The slope is close to zero or positive between 10° and 18°. This phenomenon is described by Hoerner for the swept wing configurations such as the vehicle evaluated here[41]. The reduction of pitching moment effectiveness shows up in the high lift region. Swept wing configurations generally have high angles for stall. The aircraft shows stall around 10° which corresponds to the unstable pitching moment characteristics (positive slope.) There is a reduction in pitch control effectiveness at higher angles of attack due to the outer span of the aerofoil stalling. An original goal of this project was to migrate from a conventional planform to a tailless configuration, and demonstrating adequate pitch control throughout the AOA range is a requirement. Figure 9 show that with proper CG placement, this can be achieved.

Roll moment coefficient plot, C_l *vs* α, is shown in Fig. 10. The geometric differences between the two wings resulted in a different roll moment output induced by the left and the right wing. The stiffness variation between the wings, and a larger limit cycle oscillation on the right side contributed to the left roll moment seen at angles of attack above stall. The roll moment offsets are 'trimmed' by constant voltage output to MFC actuated wings during the flight tests.

The average rolling moment coefficient was previously reported as $C_{l,ave}$ = 0·0094 for an angle-of-attack of 4·4°, or $C_{l\delta c}$ = 0·0041 /%camber for asymmetric actuation. The analysis in the previous tests, during the wind-off conditions, suggested that the rolling moments were lower than expected because the LE of the wing was actually deflecting to a lower incidence angle when the camber increased. This situation was caused by the lack of spanwise stiffness along the LE of the wings. For the previous experimentation, the reduced roll moment coefficient due to change in AOA was corrected using:

$$C_{l,corrected} = C_l + C_{L\alpha_{Exp}} \Delta\alpha \frac{A_{MFC}\, d_{MFC}}{S\, b} \quad \ldots (6)$$

where area of the wing deflected by a single MFC actuator is A_{MFC} = 0·0091m^2, and the distance from the center of the active area to the root chord is d_{MFC} = 0·31m. Once the AOA effect is removed, the roll coefficient was $C_{l,old,corrected}$ = 0·012, and the roll coefficient control derivative became $C_{l\delta c}$ = 0·0051/%.

As mentioned in the beginning of this section, the wings were modified to make a stiff LE and compliant TE to increase the change of camber for outboard section of the wing. This modification also reduced the decrease in LE incidence induced by camber change. The current configuration resulted in $C_{l,ave}$ = 0·023 for an angle-of-attack of 4°, or $C_{l\delta c}$ = 0·01 /%camber. The 145% increase from the original roll actuation was achieved due to modifications made.

https://doi.org/10.1017/S0001924000003055 Published online by Cambridge University Press

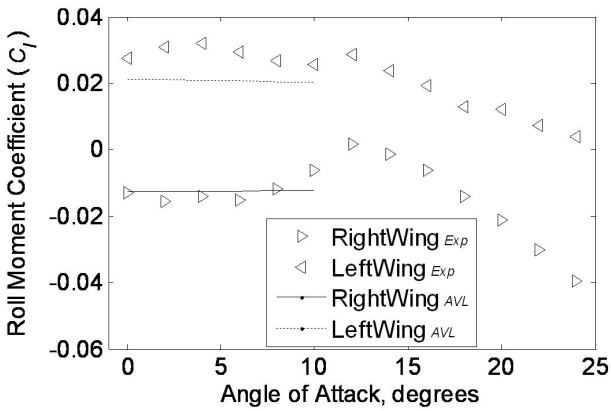


Figure 10. Roll Moment Coefficient comparison at 10·5ms^{-1}. Re_c = 1.01E5.



Figure 11. The air vehicle during its first flight on 28 February 2007.

3.4 Dynamic response analysis

One of the benefits of a single surface, laminated wing is its low inertia. The roll moment derivative resulting from roll rate, L_p , can be used to determine the settling time for a step roll command. In computing L_p, the roll moment coefficient derivative, C_{lp}, is needed. This coefficient was determined from McCormick[42] to be C_{lp} = –0·33. From Nelson[43], the time response for a step roll maneuver is:

$$\Delta p(t) = -\frac{L_{\delta c}}{L_p}(1 - e^{-t/\tau})\,\Delta\delta_c \qquad \ldots (7)$$

where $\Delta\delta_c$ is the percent change in camber, t is time, τ, L_p and $L_{\delta c}$ are:

$$\tau = -\frac{1}{L_p}, \quad L_p = \frac{C_{l_p}(b/2u)QSb}{I_x}, \quad \text{and} \quad L_{\delta c} = \frac{C_{l_{\delta c}}QSb}{I_x}. \qquad \ldots (8)$$

where u is the air velocity and moment of inertia about the roll axis is $I_x = I_{roll}$ = 1·02*10^{-2} kgm^2 . The time constant of the system becomes τ = 0·12s for the modified wings presented in this paper. The time constant represents how fast the aircraft approaches a new steady-state condition after being disturbed with a control input. The value calculated for the aircraft is small, representing a quick-responding vehicle.

The steady-state roll rate was not as high as desired, and this was due to the relatively small camber change of 2·3% being affected by the MFC patches. Theoretical steady state roll rates were determined from the non-dimensional rolling velocity, $\bar{p}$, which is given by:

$$\bar{p} = \frac{p_{ss}b}{2u} = -\frac{C_{l_{\delta c}}\Delta\delta_c}{C_{lp}} \qquad \ldots (9)$$

where p_{ss} is the steady state rolling rate, and $\Delta\delta c$ is the percent change in camber. The rolling velocity is typically used to quantify an aircraft design to meet certain minimal control requirements. For instance, fighter aircraft target a value of $\bar{p}$ = 0·09 to provide the agile handling that defines their intended use[43]. Other aircraft must meet minimum roll rates to pass the FAA airworthiness certification standards. In the case of the morphing aircraft (with modifications to the wings,) the theoretical rolling velocity is $\bar{p}$ = 0·052, which is higher than the corrected rolling velocity of $\bar{p}$ = 0·036 for the previous configuration (without modifications to the wings.)

4.0 FLIGHT TESTS

In order to validate the design, several flight attempts were made over a one month period resulting in six successful flights. Total flight time on the aircraft is estimated to be 15 minutes. Initial flight tests, shown in Fig. 11, have been conducted to trim roll and pitch characteristics. During the initial flight tests, many accidents occurred before trim points were tuned and stability was achieved. The aircraft body and the wings were virtually undamaged even after the hardest landings. It is the experience of the authors that this is not the case for vehicles with conventional control surfaces. It should be pointed out that one of the valuable lessons of these trials was in realising the resiliency of the design. Because of the thin, flexible wing, the aircraft was able to absorb impact energy sufficiently to survive approximately 30 flights, most with little or no damage to the structure.

The vehicle weight was increased due to modifications as the flight tests continued causing a higher flight speed than originally desired. Final aircraft weight was measured at 0·815kg, and this resulted in a 13ms^{-1} takeoff speed based on an initial AOA of 13°. The aircraft is hand launched at moderate running speed. Once airborne, the aircraft accelerates to 17·5ms^{-1} at a cruise AOA of 8°.

All control inputs used up to cruise conditions were conventional: the all-moving tail provided pitch input and the rudder provided lateral control based on the strong dihedral stability effect due to wing sweep. Once at cruise and with little input from the pilot, the aircraft would maintain stable flight. The elevator and rudder controls appeared very effective, and post analysis of the flight data showed that when loss of control did happen, it may have been due to the pilot working behind the lag of the rudder to affect roll through roll-yaw coupling. This caused an amplification of the dutch-roll mode, finally resulting in an irrecoverable departure.

The morphing controls were operated once the plane had reached cruise conditions. The pilot always reported not having enough control authority to fly the plane during these trials, but this may have been an assessment biased by the relatively effective rudder and short flight times. A limit cycle persisted in the wings from takeoff to landing, caused by the flexibility necessary to achieve the morphing control. The LCO experienced during flight and wind-tunnel tests is believed to reduce the effectiveness of the control surface as shown by several research papers[8,44,45]. Methods such as passive shunt damping or active vibration suppression using smart materials such as monolithic piezoceramics and piezo-composite actuators have been employed in the literature, however these techniques are not the focus of this research. The wings oscillated with a symmetrical bending/torsion mode resulting in a trailing edge peak deflection of about 20mm at a frequency of about 4Hz. This oscillation can be controlled with a feedback-controller which effectively changes the structural response of the wing.

Control inputs from the operator were of interest to demonstrate the response of the aircraft. To record the control inputs from the transmitter, a data recorder system from Eagle Tree Systems was

https://doi.org/10.1017/S0001924000003055 Published online by Cambridge University Press

used. The data logger was connected to a second receiver on ground which operated on the same frequency as the receiver on-board. Signal inputs to left and right MFC actuated wings, rudder and elevator were recorded. The recorded data was synchronised with the video of the flight. The control inputs and flight video was overlaid and post processed in one video file. On three occasions, the morphing control was successfully demonstrated. During one test, the observed roll rate came in lower than the predicted steady state roll rate from wind-tunnel data. From Equation 9, the steady-state rolling rate at 15ms^{-1} (estimated flight speed) is predicted to be p_{ss} = 1·4rads^{-1}. Based on visual observation of the flight videos, a roll rate of 0·93rads^{-1} is estimated[38] . The roll rate observed during this flight was less than predicted (from the wind-tunnel data) due to several reasons. First, the prediction was high because it was based on data from the wind-tunnel aircraft where two MFC actuators per wing were used. The fully operational aircraft used in flight tests had only one actuator per wing. Another reason is that, as previously mentioned, the aircraft went through many accidents, where the wing folded back due to the impact. While the passive composite wing was not damaged, repeated high strains induced during these impacts are believed to reduce the effectiveness slightly due to damage in PZT fibres. Finally, the limit cycle observed during the flight test also reduced the roll authority. The amplitude of the limit cycle was observed to be 20mm peak-to-peak during cruise at 8° incidence. However, only 10mm amplitude was measured during wind-tunnel tests at the 8° AOA setting. Note that the wind-tunnel tests were conducted at 10·5ms^{-1} for the purpose of reducing the limit cycle oscillation.

5.0 CONCLUSIONS AND FUTURE WORK

This study investigated the use of solid-state actuators to control the roll and pitch maneuvers of a small unmanned aircraft. The results presented here show conclusively that continuous camber change via MFC actuators a) is feasible, b) offers aerodynamic improvement over the articulated control surfaces and c) works beyond the laboratory in a flight demonstration. A 0·76m wingspan aircraft weighing about 0·8kg was designed and implemented using MFCs as actuators for the control surfaces. MFCs were employed to change the camber of the wings symmetrically and asymmetrically to cause pitch and roll moments respectively. A combination of lightweight amplifiers and converters supplied the high voltage required by the MFC actuators. All systems were powered with a Lithium-Polymer battery onboard.

The response of the MFC-actuated aircraft was quantified through wind-tunnel experimentation and flight tests. Wind-tunnel tests provided lift, drag, roll and pitch coefficients. Maximum lift coefficient of 1·06 was measured corresponding to 4·79 *L*/*D* ratio. High parasite drag caused low lift-over-drag value. Using the test data, estimates of flight performance were obtained. Non-dimensional rolling velocity of 0·052 was calculated.

The remotely piloted experimental flight vehicle was flown using two actuators in an elevator/aileron (elevon) configuration for a total flight time of 15 minutes. The design demonstrated stable aerodynamic characteristics and proved the control authority of the active materials as well as the feasibility of high voltage actuation in small unmanned aircraft. The flexible composite wing design provided excellent impact resistance. The aircraft survived approximately 30 flights, most with little or no damage to the structure. A 0·93 rads^{-1} roll rate was observed during the flight tests when the MFC actuators were used. The low moment of inertia of the composite wing design resulted in the quick-responding characteristic of the vehicle.

Establishing a wing configuration that is stiff enough to prevent an aeroelastic instability, but compliant enough to allow the range of available motion is the central challenge in developing a variable-camber wing. An optimisation between stiffness and control output can be achieved for a specific mission. One can also take advantage of the piezo-ceramic material to passively or actively tailor (and control) the aeroelastic response of the compliant wing. Authors continue research on developing novel (and passive) methods of employing piezo-composite actuators which can take advantage of aerodynamic loads to reduce control input moments and increase force outputs[34,35].

6.0 ACKNOWLEDGMENTS

Wind-tunnel tests were possible with the help of Dr William J. Devenport at the Aerospace and Ocean Engineering Department of Virginia Tech. Thanks to Dr Demetri P. Telionis at the Engineering Science and Mechanics Department for his assistance with wind-tunnel equipment. Furthermore, we would like to thank the Center for Intelligent Material Systems and Structures for sponsorship.

REFERENCES

1. LAZARUS, K.B., CRAWLEY, E.F. and BOHLMANN, J.D. Static aeroelastic control using strain actuated adaptive structures, *J Intelligent Materials, Systems and Structures*, July 1991, **2**, pp 386-410.
2. ROGLIN, R.L., HANAGUD, S.V. and KONDOR, S. Adaptive aerofoils for helicopters, 35th Structures, Structural Dynamics and Materials Conference, AIAA 1994.
3. STEADMAN, D.L., GRIFFIN S.L. and HANAGUD, S.V. Structure-control interaction and the design of piezoceramic actuated adaptive aerofoils, AIAA-1994-1747.
4. GIURGIUTIU, V., CHAUDHRY, Z. and ROGERS, C.A. Engineering feasibility of induced-strain actuators for rotor blade active vibration control, *Smart Structures and Materials '94*, Orlando, Florida, USA, 13-18 February 1994, Paper # 2190-11, SPIE Volume 2190, pp 107-122.
5. GIURGIUTIU, V. Review of smart-materials actuation solutions for aeroelastic and vibration control, *J Intelligent Material Systems and Structures*, July 2000, **11**.
6. JHA, A.K. and KUDVA, J.N. Morphing aircraft concepts, classifications and challenges, Proceedings of SPIE, 2004, **5388**.
7. BARTLEY-CHO, J.D., WANG, D.P. and WEST, M.N. Development, control and test results of high-rate, hingeless trailing edge control surface for the smart wing phase 2 wind-tunnel model, smart structures and materials 2002: Industrial and commercial applications of smart structures technologies, Proceedings of SPIE, 2002, **4698**.
8. MOSES, R.W., WEISMAN, C.D., BENT, A.A. and PIZZOCHERO, A.E. Evaluation of New Actuators in a Buffet Loads Environment, SPIE 8th Annual International Symposium on Smart Structures and Materials, 2001, Newport Beach, CA, USA.
9. CADOGAN, D., SMITH, T., LEE, R., SCARBOROUGH, S. and GRAZIOSI, D. Inflatable and Rigidizable wing components for unmanned aerial vehicles, AIAA 2003-6630, 44th AIAA/ASME/ASCE/AHS/ASC Structures, Structural Dynamics and Materials Conference, April, 2003, Norfolk, VA, USA.
10. CADOGAN, D., SMITH, T., UHELSKY, F. and MACKUSICK, M. Morphing inflatable wing development for compact package unmanned aerial Vehicles, AIAA-2004-1807, 45th AIAA/ASME/ASCE/AHS/ASC Structures, Structural Dynamics and Materials Conference, April 2004, Palm Springs, CA, USA.
11. MURRAY, J., PAHLE, J., THORNTON, S., FRACKOWIAK, T., MELLO, J. and NORTON, B. Ground and Flight Evaluation of a Small-Scale Inflatable-Winged Aircraft, AIAA 2002-0820, 40th AIAA Aerospace Sciences Meeting and Exhibit, Reno, NV, USA, 14–17 January 2005.
12. SIMPSON, A. and JACOB, J. Aerodynamic control of an inflatable wing using wing warping, 35th AIAA Fluid Dynamics Conference and Exhibit, 6 - 9 June 2005, Toronto, Ontario Canada, AIAA 2005-5133
13. LESIEUTRE, G. and DAVIS, C. Can a coupling coefficient of a piezoelectric device be higher than those of Its active material? *J Intelligent Materials Systems and Structures*, 1997, **8**, (10), pp 859-867.
14. VOS, R., DEBREUKER, R., BARRETT, R. and TISO, P. Morphing wing fight control via post-Buckled precompressed piezoelectric actuators, *J Aircr*, **44**, (4), July-August 2007, pp 1060-1069.
15. SEIGLER, T.M., NEAL, D.A., BAE, J.S. and INMAN, D.J. Modeling and flight control of large-scale morphing aircraft, *J Aircr*, **44**, (4), July–August 2007
16. GLEZER, A., AMITAY, M. and HONOHAN, A. Aspects of low- and high-frequency actuation for aerodynamic flow control, *J AIAA*, **43**, (7), 2005, pp 1501 – 1511.

https://doi.org/10.1017/S0001924000003055 Published online by Cambridge University Press

17 PERN, N.J., JACOB, J. and LEBEAU, R. Characterization of zero mass flux flow control for separation control of an adaptive aerofoil, AIAA Paper 2006-3032, 36th Fluid Dynamics Conference, June 2006.

18. RAMAKUMAR, K., and JACOB, J. Flow control and lift enhancement using plasma actuators, AIAA Paper 2005-4635, 35th Fluid dynamics Conference, June 2005.

19. ROGERS, E., SCHWARTZ, A. and ABRAMSON, J. Applied aerodynamics of circulation control aerofoils and rotors, annual forum proceedings of the American Helicopter Society, 1985, **2**, (41), pp 479 – 490.

20· ACHARYA, M., EMO, S., BUGAJSKI, D. AND WILLIAMS, D. Smart vanes for UCAV engine applications, 2nd AIAA Flow Control Conference, 28 June – 1 July 2004, Portland, Oregon, USA, AIAA 2004-2516.

21. SANTHANAKRISHNAN, A., PERN, N.J., RAMAKUMAR, K., SIMPSON, A. and JACOB, J.D. Enabling Flow Control Technology for Low Speed UAVs, Infotech@Aerospace 26 – 29 September 2005, Arlington, Virginia, USA, AIAA 2005-6960.

22. GOMES, L.D., CROWTHER, W.J. and WOOD, N.J. Towards a practical piezoceramic diaphragm based synthetic jet actuator For high subsonic applications – effect of chamber and orifice depth on actuator peak Velocity, 3rd AIAA Flow Control Conference, 5–8 June 2006, San Francisco, California, USA, AIAA 2006-2859.

23. PATEL, M.P., NG, T.T., VASUDEVAN, S., CORKE, T.C. and HE, C. Plasma actuators for hingeless aerodynamic control of an unmanned air vehicle, *J Aircr*, **44**, (4), July–August 2007

24. IFJU, P.G., JENKINS, D.A., ETTINGER, S., LIAN, Y., SHYY, W. and WASZAK, M.R. flexible-wing-based micro air vehicles, AIAA Annual Conference, AIAA 2002~0705. January 2002.

25. WASZAK, M.R., JENKINS, L.N. and IFJU, P.G. Stability and control properties of an aeroelastic fixed wing micro aerial vehicle, AIAA 2001~4005.

26. ALBERTANI, R., STANFORD, B., HUBNER, J.P., LIND R. and IFJU, P. Experimental Analysis of deformation for flexible-wing micro air vehicles, 2005 AIAA SDM Conference, Austin, TX, USA, May 2005.

27. TORRES, G.E. Aerodynamics of Low Aspect Ratio Wings at Low Reynolds Numbers with Applications to Micro Air Vehicle Design, Ph.D. Dissertation, Aerospace and Mechanical Engineering Dept., University of Notre Dame, Indiana, USA, April 2002.

28. GARCIA, H.M., ABDULRAHIM, M. and LIND, R., Roll control for a micro air vehicle using active wing morphing, AIAA 2003~5347.

29. Kim, D.K. and Han, J.H. Smart flapping wing using macro-fiber composite actuators, proceedings of SPIE Vol. **6173** 61730F, 2006, pp 1-9.

30· WILKIE, W.K., BRYANT, G.R. and HIGH, J.W. Low-cost piezocomposite actuator for structural control applications, SPIE 7th Annual International Symposium on Smart Structures and Materials, 2000, Newport Beach, CA, USA.

31. HIGH, J.W. and WILKIE, W.K. Method of fabricating NASA-standard macro-fiber composite piezoelectric actuators, NASA/TM-2003-212427, ARL-TR-2833.

32. HAGOOD, N.W., KINDEL, R., GHANDI, K. and GAUDENZI, P. Improving transverse actuation using interdigitated surface electrodes, SPIE Paper No. 1917-25, 1993 North American Conference on Smart Structures and Materials, Albuquerque, NM, USA, pp 341-352.

33. WILLIAMS, R.B. Nonlinear Mechanical and Actuation Characterization of Piezoceramic Fiber Composites, PhD. Dissertation, Mechanical Engineering Dept., Virginia Tech, Blacksburg, VA, USA, 22 March 2004.

34. BILGEN, O., KOCHERSBERGER, K. and INMAN, D.J. An experimental and analytical study of a flow vectoring aerofoil via macro-fiber-composite actuators, Proc. of SPIE, **6930**, SPIE Smart Structures and NDE 2008, San Diego, California, USA, 9-13 March 2008.

35. BILGEN, O., KOCHERSBERGER, K. and INMAN, D.J. A novel aerodynamic vectoring control aerofoil via macro-fiber-composite actuators, AIAA-2008-1700, 49th AIAA/ASME/ASCE/AHS/ASC Structures, Structural Dynamics and Materials Conference, Schaumburg, Illinois, USA, 7-10 April 2008.

36. BILGEN, O., KOCHERSBERGER, K., DIGGS, E.C., KURDILA, A.J. and INMAN, D.J. Morphing Wing Micro-Air-Vehicles via Macro-Fiber-Composite Actuators, AIAA-2007-1785, 48th AIAA/ASME/ASCE/AHS/ASC Structures, Structural Dynamics and Materials Conference, Honolulu, Hawaii, USA, 23-26 April 2007.

37. DRELA, M., AVL 3.26 User Primer, [http://web.mit.edu/drela/Public/web/avl/avl_doc.txt.]

38. BILGEN, O., KOCHERSBERGER, K., DIGGS, E.C., KURDILA, A.J. and INMAN, D.J. Morphing wing aerodynamic control via macro-fiber-composite actuators in an unmanned aircraft, AIAA-2007-2741, AIAA Infotech @ Aerospace Conference, Rohnert Park, California, USA, 7-10 May 2007.

39. AIAA Standard on assessment of experimental uncertainty with application to wind-tunnel testing, S-071A-1995, AIAA, New York, USA, 1995.

40. KOCHERSBERGER, K., WALD, Q. and HYDE, K. An experimental and analytical evaluation of the 1911 Wright Bent End Propeller, Paper No. 2000-4122, 18th Applied Aerodynamics Conference, AIAA, Denver, CO, USA, 14 – 17 August 2000·

41. HOERNER, S.F. *Fluid-Dynamic Lift*, published by Mrs LISELOTTE A. Hoerner, 1975, (XVI).

42. MCCORMICK, B. *Aerodynamics, Aeronautics and Flight Mechanics*, 2nd Ed, John Wiley and Sons, New York, NY, USA, 1994, p 527.

43. NELSON, R.C. *Flight Stability and Automatic Control*, 2nd Ed, McGraw Hill, Boston, MA, USA, 1998, p 182.

44. HEEG, J. Analytical and experimental investigation of flutter suppression by Piezoelectric Actuation, NASA. Technical Paper 3241, Langley Research Center, Hampton, Virginia, USA, 1993.

45. HEEG, J., MILLER, J.M. and DOGGETT JR., R.V. Attenuation of empennage buffet response through active control of damping. using piezoelectric material, NASA Technical Memorandum 107736, Langley Research Center, Hampton, Virginia, USA, 1993.

https://doi.org/10.1017/S0001924000003055 Published online by Cambridge University Press